Exoplanet Characterisation Observatory (EChO)

Assessment Phase Payload Study

EChO Pointing Jitter Impact on Photometric Stability

ECHO-TN-0003-UCL

Issue 1.4

Prepared by: Ingo P. Waldmann, Enzo Pascale Date: 26/11/2013

Checked / Approved by: Bruce Swinyard, Paul Eccleston Date: 26/11/2013

DOCUMENT CHANGE DETAILS

Issue	Date	Page	Description Of Change	Comment
0.1	29/08/13		Initial document	
0.2	09/09/13	16	Implemented comments by E. Pascale	
1.0	11/09/13	All	Updated with further comments and feedback. Document released for PRR datapack.	
1.1	19/09/13	10-11	Updated figures 6-9	
1.2	25/09/13		Corrections to the text	
1.3	26/11/13	11-12	Updated figures 6-9, removed Appendix A	
1.4	10/12/13	2	Updated table captions	

DISTRIBUTION LIST

EChO Payload Consortium				External	
Co-PIs / Science Team Coordinators		Study Engineering Team Working Group Leads		European Space Agency	
✓	Giovanna Tinetti	✓	Paul Eccleston		Luigi Colangeli
	Hans Ulrik Nørgaard-Nielsen	✓	Ranah Irshad	✓	Kate Isaak
	Jean-Philippe Beaulieu		Emanule Pace	✓	Ludovic Puig
	Paul Hartogh		Gianluca Morgante	✓	Martin Linder
	Giusi Micela		Berend Winter		Roger Walker
	Ignasi Ribas		Marc Ferlet		Matthias Ehle
✓	Bruce Swinyard		Mercedes Lopez-Morales		Nicola Rando
	Mark Swain		Vince Coudé du Foresto		
	Tanya Lim		Alberto Adriani		
	Neil Bowles		Jean-Michel Reess		
✓	Enzo Pascale	✓	Marc Ollivier		
	Gillian Wright		Gonzalo Ramos Zapata		
	Graziella Branduardi-Raymont		Neil Bowles		
	Marc Ollivier	**Other Engineering Team**			
	Pierre-Olivier Lagage		*As necessary for doc*		
	Vince Coudé du Foresto				
	Athena Coustenis				
	Emanuele Pace				
	Giuseppe Piccioini				
	Giuseppe Malaguti				
	Alessando Sozzetti				
	Maria Rosa Zapataro Osorio				
	Mercedes Lopez-Morales				
	Enric Palle				
	Christopher Jarchow				
	Denis Grodent				
	Allan Hornstrup				
	Geza Kovacs				
	Pierre Drossart				
	T Encrenaz				
	L Fletcher				
	D Pinfield				
	J Cho				
	F Forget				
✓	I Waldmann				
✓	P Deroo				
	I Mueller-Wodarg				
	F Selsis				
	O Grasset				
	L Stixrude				
	T Guillot				
	Others…				

TABLE OF CONTENTS

1 PREAMBLE

1.1 SCOPE

This document covers the pointing jitter stability of EChO.

1.2 PURPOSE

We are currently investigating the impact of pointing jitter on the signal to noise ratio (SNR) of the final spectrum observed by EChO. This is in light of three spacecraft stabilisation methods being currently discussed: 1) Cold gas (30 mas-rms jitter), 2) Reaction wheels opt. 1 (50 mas-rms jitter), 3) Reaction wheels opt. 2 (130 mas-rms jitter).

We have here considered the two limiting cases: 1) photon noise limited 55 Cnc e and 2) detector noise limited GJ1214b (as specified in the EChO-MRD).

1.3 APPLICABLE DOCUMENTS

AD #	APPLICABLE DOCUMENT TITLE	DOCUMENT ID	ISSUE / DATE
1			
2			
3			

1.4 REFERENCE DOCUMENTS

RD #	REFERENCE DOCUMENT TITLE	DOCUMENT ID	ISSUE / DATE
1	EChO - MRD	SRE-PA/2011.038	3 -14/09/12
2	EChOSim URD	ECHO-TN-001-CF-URD	3.0
3	EChOSim SRD	ECHO-RN-002-CF-SRD	2.0

2 INTRODUCTION

In this tech note we consider the effect of pointing instabilities on the photometric accuracy of EChO.The high and low frequency jitter of the telescope can give rise to various effects affecting the photometric stability of a time series measurement:

1) Slit losses: Stellar flux may be lost through temporary misalignment of the beam with the slit of the classical slit fed spectrograph modules. This is not deemed a problem with EChO due to the large slit widths selected in each optical module.
2) Vignetting at fibre-stops: Similarly to slit losses, flux may be lost at fibre fed instruments due to vignetting.
3) Inter-pixel variations: through jittering the telescope, the point spread function (PSF) of the dispersed spectrum on the detector focal plane can and will shift in the spatial and spectral directions. Here gain variations between pixels as well as overall flat-fielding effects will give rise to time varying flux readings due to the spatial shifting of the stellar flux on the detector plane.
4) Intra-pixel variations: Sub-pixel quantum efficiency (QE) variations have a similar effect on time series noise as inter-pixel variations do. For instruments such as Spitzer/IRS, Spitzer/IRAC, Hubble/NICMOS, Hubble/WFC3, these variations (both inter and intra-pixel) are the main source of systematic error.

A high pointing stability of the spacecraft is desirable but a perfect pointing is not always required if the systematic photometric effects can be mitigated in careful post analysis. Such an approachopens the possibility to investigate different systems of pointing stabilisations.

We investigate three potential systems for the stabilisation of the spacecraft pointing: Cryogenic Jets (also referred to as 'cold gas option' in the text, as well as two reaction wheel options of varying accuracy (referred to as options 1 and 2 in the text).

Figure 1 is taken from the EChO MRD (figure 8) detailing the relative noise requirements of EChO as a function of wavelength.

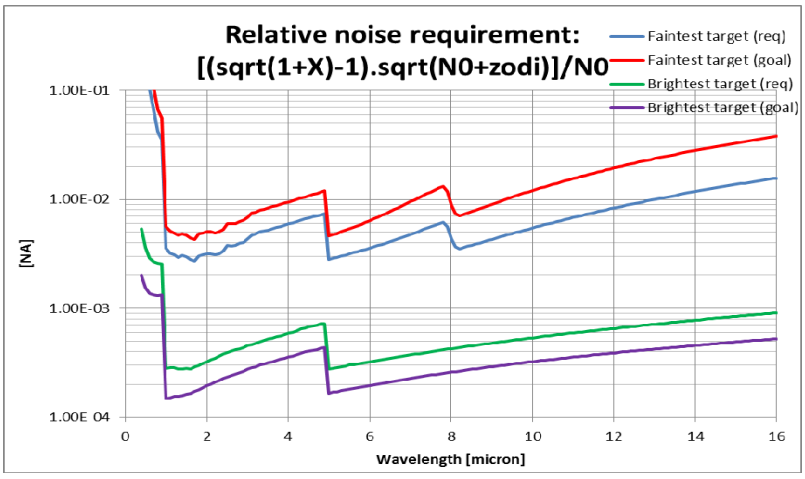

Figure 1: from ESA-MRD (figure 8) showing the relative noise requirements fro EChO as a function of wavelength.

Table 1: Simulations for the Faint Source object (MRD: R-PERF-090) for expected jitter (private communication with ESA study team).

Type	Amplitude	Spectral density	EChOSim Nodes
Cryo Jets (Faint source)	RPE: 30 masc-rms 1–10 Hz PRE: 20 mas-rms 0.028–4 mHz	9 masc/rt(Hz) 317 masc/rt(Hz)	f = 2.5e-5, 2.8e-5, 4e-3, 4.4e-3, 0.9, 1, 10, 11
			p = 1e-10, 317, 317, 1e-10, 1e-10, 9, 9, 1e-10
R. Wheel Opt. 1 (Faint source)	RPE: 50 masc-rms, 1 – 300 Hz PRE: 20 mas-rms 0.028–4 mHz	2.9 masc/rt(Hz) 317 masc/rt(Hz)	f = 2.5e-5, 2.8e-5, 4e-3, 4.4e-3, 0.9, 1, 300, 330
			p = 1e-10, 317, 317, 1e-10, 1e-10, 2.9, 2.9, 1e-10
R.Wheel Opt. 2 (Faint source)	RPE: 130 masc-rms 1- 300 Hz PRE: 20 mas-rms 0.028–4 mHz	7.5 masc/rt(Hz) 317 masc/rt(Hz)	f = 2.5e-5, 2.8e-5, 4e-3, 4.4e-3, 0.9, 1, 300, 330
			p = 1e-10, 317, 317, 1e-10, 1e-10, 7.5, 7.5, 1e-10

Table 2: Simulations for the Bright Source object (MRD: R-PERF-110) for expected jitter (private communication with ESA study team).

Type	Amplitude	Spectral density	EChOSim Nodes
Cryo Jets (Bright source)	RPE: 20 masc-rms 1–10 Hz PRE: 10 mas-rms 0.028–4 mHz	6 masc/rt(Hz) 159 masc/rt(Hz)	1 f = 2.5e-5, 2.8e-5, 4e-3, 4.4e-3, 0.9, 1, 10, 11
			p = 1e-10, 159, 159, 1e-10, 1e-10, 6, 6, 1e-10
R. Wheel Opt. 1 (Bright source)	RPE: 33 masc-rms, 1 – 300 Hz PRE: 20 mas-rms 0.028–4 mHz	1.9 masc/rt(Hz) 317 masc/rt(Hz)	2 f = 2.5e-5, 2.8e-5, 4e-3, 4.4e-3, 0.9, 1, 300, 330
			p = 1e-10, 317, 317, 1e-10, 1e-10, 1.9, 1.9, 1e-10
R.Wheel Opt. 2 (Bright source)	RPE: 100 masc-rms 1- 300 Hz PRE: 20 mas-rms 0.028–4 mHz	5.8 masc/rt(Hz) 317 masc/rt(Hz)	2.1.1.3 f = 2.5e-5, 2.8e-5, 4e-3, 4.4e-3, 0.9, 1, 300, 330
			p = 1e-10, 317, 317, 1e-10, 1e-10, 5.8, 5.8, 1e-10

2.2 DEFINITIONS

In this tech note we will consider two jitter types:

1) **RPE** (Relative performance error), defining the high frequency (> 1 Hz), unresolved jittercomponent.
2) **PRE** (Performance reproducibility error), defining the low frequency (< 1 Hz), resolved PSF drifting due to pointing jitter.
3) **MPE** (Mean performance error), is the overall offset (in time series, the flux offset) between two or more observation windows.

The various error definitions in relation to plotted time series are shown in figure 1.

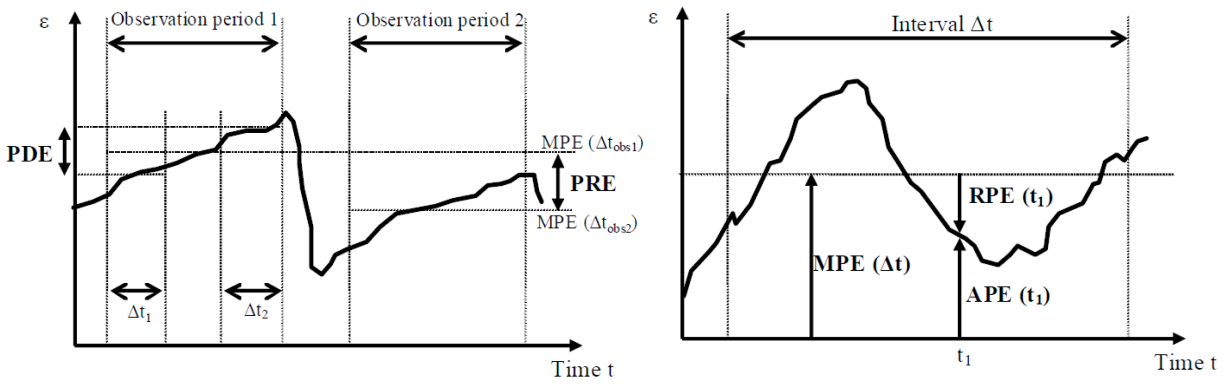

Figure 1:showing noise definitions on two time series plots. **MPE** = mean performance error; **APE** = absolute performance error; **RPE** = relative performance error; **PRE** = performance reproducibilityerror; **PDE** = performance drift error (source of figures:http://www.summerschoolalpbach.at/docs/2012/lectures/Erd_Alpbach_2012.pdf; definitions: ESA-URD).

2.3 JITTER MODES

Table 3: PRE and RPE amplitudes considered for the three cases: Cryo Jets, Reaction Wheel Option 1, Reaction Wheel Option 2. The masc-rms values are translated into spectral densities and EChOSim spectral nodes.

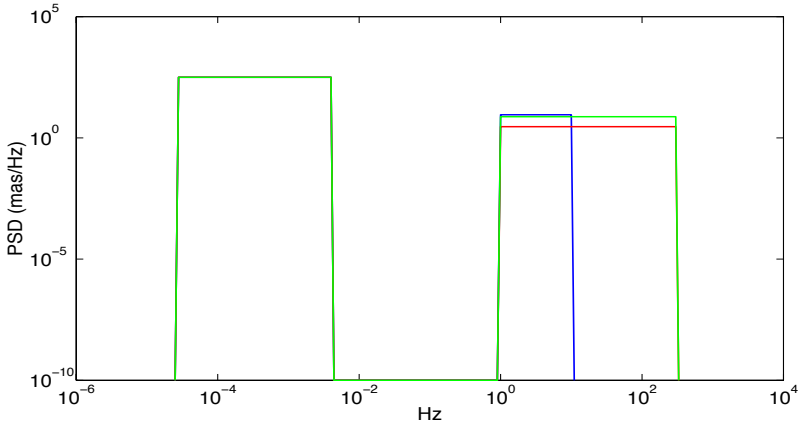

Figure 2: shows Power spectrum of the three jitter modes for the faint target (tabulated in table 1): Blue: Cryo Jets; Red: Reaction Wheel Option 1; Green: Reaction Wheel Option2.

2.4 ECHOSIM

EChOSim is an end-to-end simulator of the EChO mission (see EChOSim URD & SRD). In its latest version, 3.0, we have implemented the possibility to jitter the point spread function (PSF) along the spatial direction of the focal plane. The jitter power spectrum is defined in EChOSim via the use of spectral nodes (see table 1) in the parameter file.

We refer the reader to section 4.1 (and the EChOSim URD) for jitter implementation details.

2.5 SIMULATION OVERVIEW

We simulated the impact of the pointing jitter on all EChO channels (VNIR, SWIR, MWIR, LWIR).

2.5.1 VNIR

In the current design considerations the VNIR focal plane is fibre fed. This result in a static PSF on the detector but the jitter on the fibre stops needs to be simulated. Whilst EChOSim includes a fibre fed VNIR implementation, we simulate the jitter on the fibre stops in a separate study presented in section 3.

2.5.2 SWIR/MWIR/LWIR

For wavelengths long wards of 2.5 µmwe follow the modelling approach by Deroo et al. (2012)[1]and simulated the effect of pointing jitter along the spatial axis of the focal plane using EChOSim (section 4).

2.5.3 PSF Breathing

The effect of PSF breathing which is a time-varying PSF width and associated instrumental photometric-gain variation is simulated and discussed in section 5.

[1]Deroo, P., Swain, M. R., Greene, T. P., 2012, 'Optimizing Instrument Stability for Exoplanet Spectroscopy'

3 VNIR

The simulations deriving the rms noise contribution for the fibre fed VNIR channel are performed outside the EChOSim code. The methodology is briefly outlined in section 3.1 and the simulations for two wavelength(0.8µm and 2.5 µm) are shown in section 3.2.1 and 3.2.2. The overall noise in terms of e^-/spectral-bin was calculated using flux throughputs derived from EChOSim in section 3.2.3.

3.1 DESCRIPTION OF SIMULATIONS

- Simulations are done in IDL outside EChOSim
- PSF at fibre input from max simulations Marc F. This is a representative PSF from a telescope which is diffraction limited at 3 microns and meets the telescope performance requirements agreed for the EID-A. The distribution of errors between Zernike parameters is arbitrary, but is based on previous experience of such telescope systems and is distributed between high and low frequency errors.
- Simulation estimates the RMS power loss due to APE-induced random vignetting. This is done as a function of MPE from 0 to 600mas.
- The PSF at fibre input is multiplied by a circular top-hat (diameter 50µm) offset by the MPE + RPE(t).

$$S(t) = \langle PSF \times TopHat\ (MPE + RPE(t))\rangle_{ls}$$

- The resulting photometric noise is estimated as

$$\sigma_{ph} = stdev[S(t)]$$

- To obtain an equivalent noise in e^-s^{-1} per resolution element P, multiply σ_{ph} by the detected point-source signal

3.2 SIMULATION

3.2.1 Blue edge: 0.8 µm

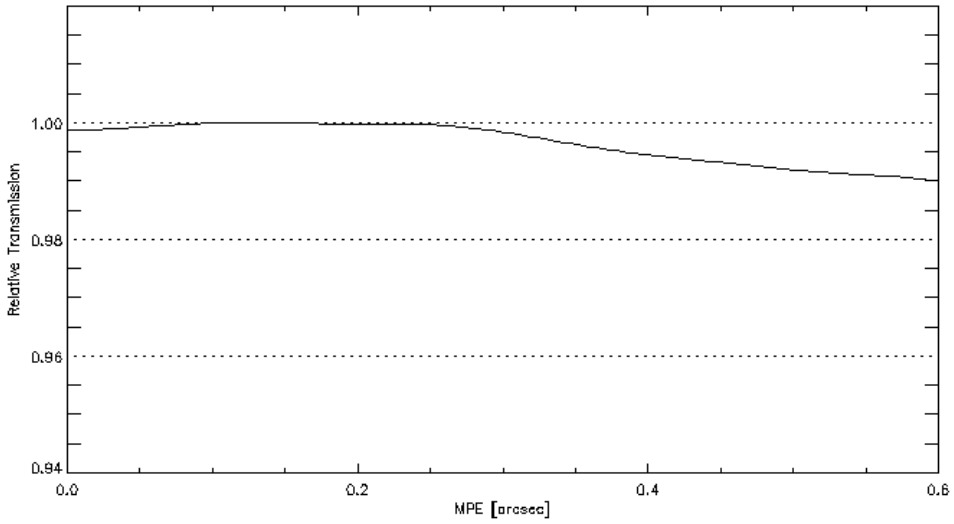

Figure 2: shows the variation in the fraction of transmitted power vs MPE. It is normalised to unity at maximum.

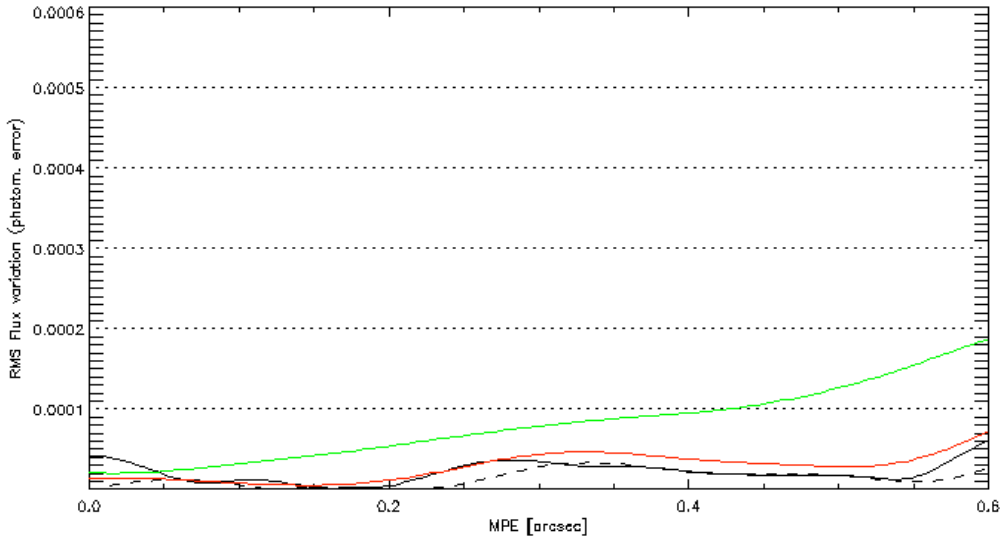

Figure 3: shows the photometric error, $\sigma_{ph,}$ in one second integration time. The black, red and green solid lines are for a jitter induced by cold gas, reaction wheel opt 1 and reaction wheel opt 2, respectively.

3.2.2 Red edge:2.5 µm

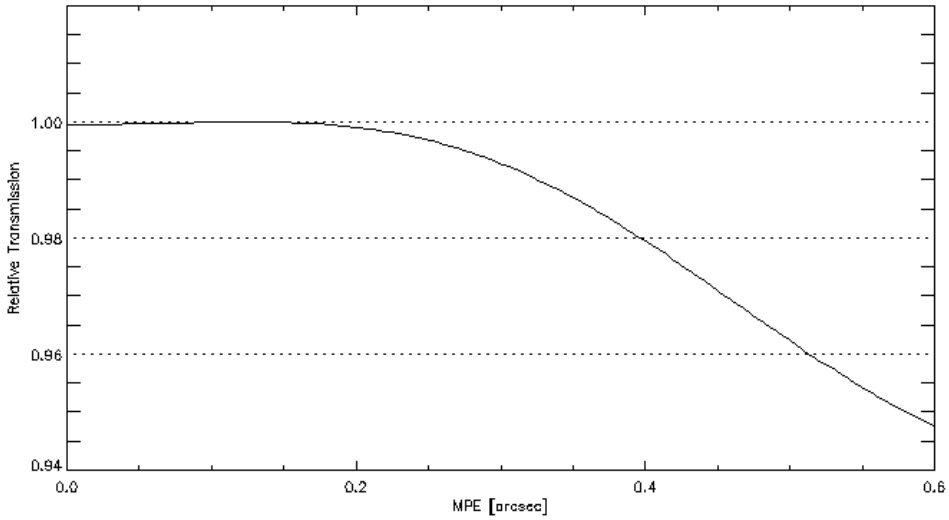

Figure 4: shows the variation in the fraction of transmitted power vs MPE. It is normalised to unity at maximum.

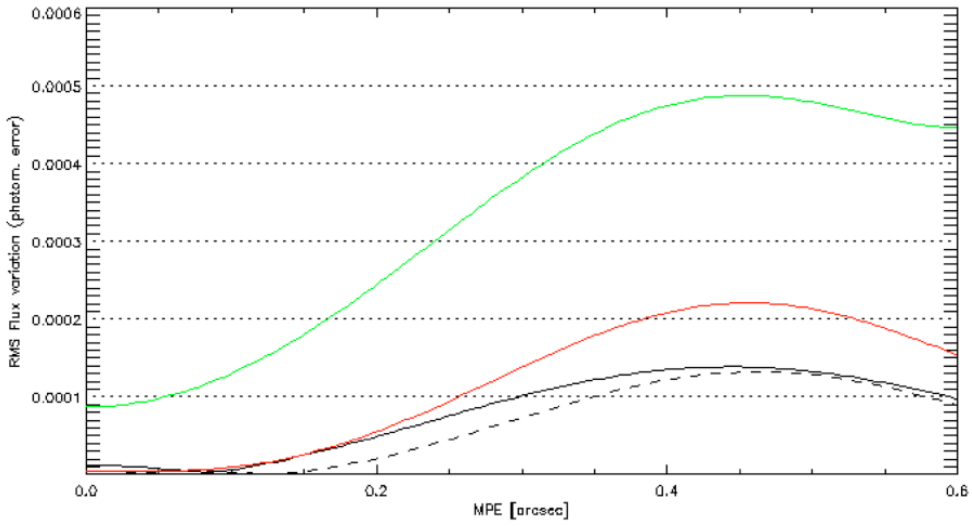

Figure 5: shows the photometric error, $\sigma_{ph,}$ in one second integration time. The black, red and green solid lines are for a jitter induced by cold gas, reaction wheel opt 1 and reaction wheel opt 2, respectively.

3.2.3 Translation into noise in e^-/spectral-bin

The rms power loss presented in figures 3 and 5 affects the detected signal from the point source observed (here referred to as Q_{point} with the units $e^-s^{-1}spec\_bin^{-1}$). Note that Q_{point} is the detected signal and includes QE and optical efficiencies.

We hence have as total error (standard deviation) in one second:

$$\sigma = \sigma_{ph} \times Q_{point}$$

Table 1 shows this error term at different wavelengths and assuming different pointing jitter values. The worst case (i.e. the max(σ_{ph}) is used).

Table 4: showing the maximum standard deviation, max(σ_{ph}), in units of e^-/spectral_bin at 0.8 µm and 2.5 µm for the brightest and faintest sources in one second of integration. Cold Gas, Reaction Wheel Opt. 1 and Reaction Wheel Opt. 2 are considered for both targets and wavelengths. The bottom two rows indicate the maximum allowed variance and standard deviation (in e^-/spectral_bin).

Wavelength	Brightest Req.			Faintest Req.		
	Cold Gas	R. Wheel 1	R. Wheel 2	Cold Gas	R. Wheel 1	R. Wheel 2
0.8 µm	5	5	14	0.02	0.02	0.06
2.5 µm	17	28	62	0.2	0.3	0.7
Var. allowed	38300	38300	38300	611	611	611
Stdev. allowed	195	195	195	24	24	24

3.3 SUMMARY & INTERPRETATION

As reported in table 1, the overall noise due to telescope jitter is well within the allocated noise budget. For the brightest star considered by the MRD, the pointing jitter noise contribution varies from ~8.7% (for the Cold Gas option) to ~31.8% (for the Reaction Wheel Opt. 2) of the total allowed noise budget. The resulting variances are summarised in table 2. Photometric instabilities due to jitter are negligible for faint targets in the VNIR.

Overall there are no constraints on pointing stability with respect to the VNIR channel.

4 SWIR/MWIR/LWIR

The all wavelengths beyond 2.5 µmare modelled using the Jitter simulation module in EChOSim 3.0. Whilst for more details we refer the reader to the EChOSim URD/SRD, we briefly outline the implementation of the spatial pointing jitter.

Note[2]: We model a spectroscopic observation and limit the analysis to the photometric impact of instrument changes along the cross-dispersion direction (i.e. the spatial axis). Changes along the spectral axis will have a significantly lower impact on the photometric noise level because the electron count difference is modulated by the difference in flux between adjacent spectral channels.

4.1 METHODOLOGY

4.1.1 Jitter implementation

EChOSim uses the following approximation to simulate the response of a pixel in the detector focal plane array to illumination from a point-like source

$$Q_{ij}(t) = \simeq p_{ys}(y_j, \lambda_i) \int_{-\infty}^{+\infty} F_{\lambda,t}\, p_{xs}(LD(\lambda - \lambda_i))\, d\lambda$$

The indices i and j define one pixel in the focal plane array. The sampled point spread function x and y cross sections, p_{xs} and p_{ys}, depend from the wavelength sampled by the detector. The linear dispersion law connects the physical pixel coordinate to the wavelength sampled by the detector:

$$x_i = LD(\lambda_i - \lambda_0) + x_0$$

The pointing jitter in the spatial direction is expressed by a second order Taylor expansion in the *y* coordinate:

$$Q^J_{ij}(t) = Q_{ij}(t)\left\{1 + \frac{1}{p_{ys}(y_j, \lambda_j)}\left[\left.\frac{\partial p_{ys}}{\partial y}\right|_{y=y_j} \delta y_s(t) + \frac{1}{2}\left.\frac{\partial^2 p_{ys}}{\partial y^2}\right|_{y=y_j} \delta y_s^2(t)\right]\right\}$$

$$Q_{ij}(t)\left\{1 + \frac{f_{eff}}{p_{ys}(y_j, \lambda_j)}\left[\left.\frac{\partial p_{ys}}{\partial y}\right|_{y=y_j} \delta\theta_s(t) + \frac{f_{eff}^2}{2}\left.\frac{\partial^2 p_{ys}}{\partial y^2}\right|_{y=y_j} \delta\theta_s^2(t)\right]\right\}$$

The jitter is $\delta y_s(t) = f_{eff}\delta\theta_s(t)$ and $\delta\theta_s(t)$ is a random variable, which is identical for each detector array in each array in each EChO focal plane (i.e. correlated jitter).

The jitter $\delta\theta_s(t)$ timeline is generated given a refrence power spectral density(PSD) taken from table 1.

Note: Pointing-jitter affects the signal as the ramp is sampled during each non-destructive-reading (NDR). EChOSim does not implement NDR and follow-up-the-ramp. EChOSim only implements the last reading before the JFET reset.. We hence take the average $< \delta\theta_s(t) >$ and $< \delta\theta_s^2 >$ over the sampling interval. This effectively is the time between two reset events.

[2] following:Deroo, P., Swain, M. R., Greene, T. P., 2012, 'Optimizing Instrument Stability for Exoplanet Spectroscopy'

4.1.2 PRE detrending

The current PRE detrending is performed in the observation pipeline delivered with EChOSim. The Jitter module in EChOSim simulates centroiding information of the fine guidance sensor (FGS) in the spatial direction at a frequency of 1 Hz.

EChOSim takes the original jitter time-series,$\delta y_s(t)$,derived from table 1 and integrate to 1 Hz temporal sampling. We add a 10 masc-rms Gaussian error to the FGS time series.

The simulated 1 Hz FGS time series is passed to the observation pipeline where it is downsampled to the nominal total integration time to yield the de-trending spatial displacement time series, $\delta y_{detrend}(t)$. Note that NDRs are not considered.

The observation pipeline calculates a Gaussian PSF, offset by $\delta y_{detrend}(t)$ from its original position and convolves this with the pixel response, *PR*, assumed by EChOSim.

$$PSF_{shift}(t) = PR \otimes G(x_0 + \delta y_{detrend}(t), \sigma)$$

$PSF_{shift}(t)$ is used to optimally extract the one dimensional spectra from the two dimensional focal plane illuminations produced by EChOSim. No further de-trending steps are implemented.

4.2 INITIAL CONSIDERATIONS

Table 1 summarises the currently assumed specifications. These were translated into power-spectra of the pointing jitter and fed into EChOSim (figure 1). Viewing figure 1 we can immediately note the following:

1. The power-spectrum is assumed to be Gaussian with a high-frequency cut off.

2. The power spectral density (psd) is higher for the cold gas option (at low frequencies) than reaction wheel 1 and similar to reaction wheel 2.

These two observations are important characteristics of the jitter model assumed. Given a maximum sample speed of 1 Hz, jitter at higher frequencies than that (if the power-spectrum is Gaussian) will not result in systematic drifts but cause an enlargement of the PSF. This needs to be accounted for at the spectral reduction stage. Jitter at low frequencies is potentially observed and results in time-correlated systematics in the final derived time series. At these low frequencies ($\leqslant$ 1 Hz), the reaction wheel option 1 has the lowest spectral density of the three systems proposed and promises a higher stability at these critically low frequencies.

4.3 RPE NOISE

We have initially only considered the RPE noise of the three jitter modes. This high frequency jitter is not resolved by individual exposures (or ramp reads) but the integrated jitter constitutes a ‘smearing’ of the PSF across the focal plane. As described in section 4.2, we are most sensitive to high PSDs at low frequencies and do not necessarily find the cryo-jet option favourable as the spectral window over which the overall 30 masc-rms is spread is smaller. Figures 6 and 7 show the RPE jitter noise for both, the photon noise (55 Cnc e) and detector noise (GJ1214b) limited cases respectively.

Note: Given the specifications in table 1, we can assume (and indeed find) that the differing RPE values for the various options constitute the main source of differences in following simulations (PRE is fixed at 20mas-rms for all three options).

In the plots presented in section 4.3 and 4.4 we define the relative jitter noise contribution (following figure1) as follows:

$$X = \frac{\sigma^2_{jitter}}{(F_{star} + F_{zodi})}$$

where *X* is the excess noise variance due to jitter (following R-PERF-350 of the MRD). The R-PERF-350 requirement on *X* is X< 1 at wavelengths shorter than 1μm, and X < 0.3 at wavelengths longer than 1μm

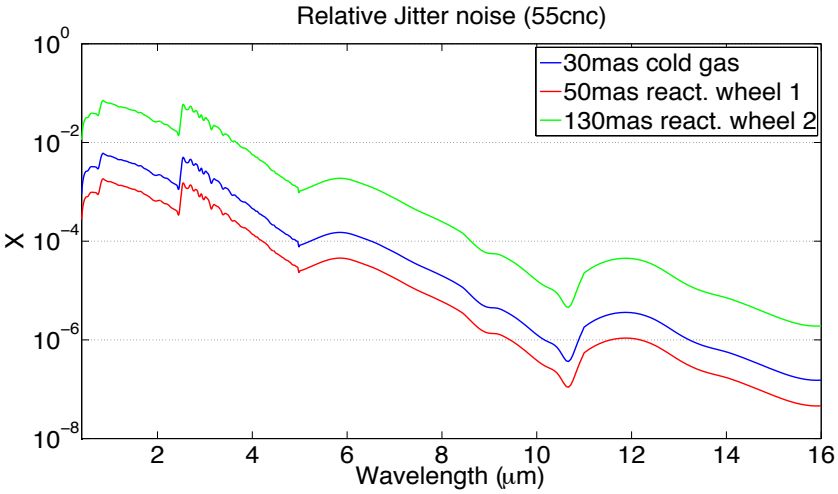

Figure 6: Excess noise variance as function of wavelength for the photon noise limited case 55 Cnc e. Here only RPE noise is considered. Blue: Cold Gas; Red: Reaction Wheel Option 1; Green: Reaction Wheel option 2.

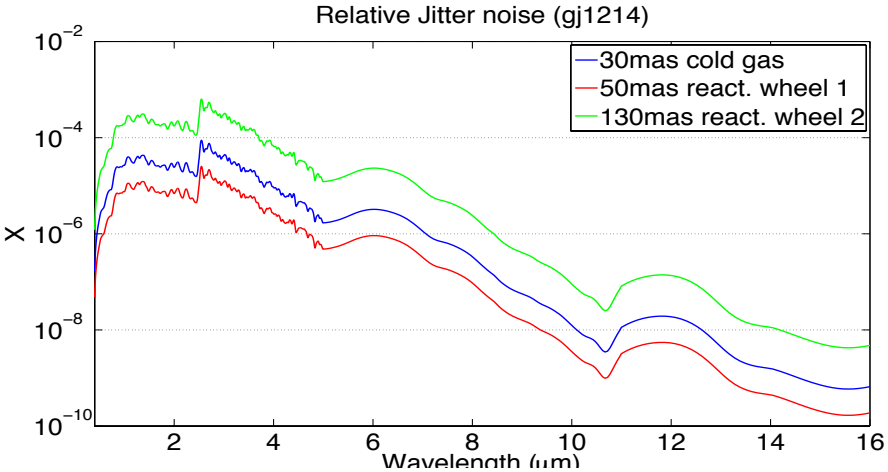

Figure 7: Excess noise variance as function of wavelength for the detector noise limited case GJ1214b. Here only RPE noise is considered. Blue: Cold Gas; Red: Reaction Wheel Option 1; Green: Reaction Wheel option 2.

4.4 RPE AND PRE NOISE

PRE noise (for the purpose of the simulations presented here) is considered to be the same for all three simulation cases (see table 1 and figure 1). Hence, the main differences between the three different jitter modes are dominated by the change in RPE noise (see section 4.2).

What is expected a similar result to figures 6 and 7 with an increased noise floor assuming a constant de-trending efficiency. This is true for the photon noise limited case (figure 8) but not so for the detector noise limited case (figure 9) where we find a much similar jitter levels for all three modes post decorrelation.

For both cases, using this simplistic de-trending approach, we obtain about a factor of 3 improvement over non-detrended data.

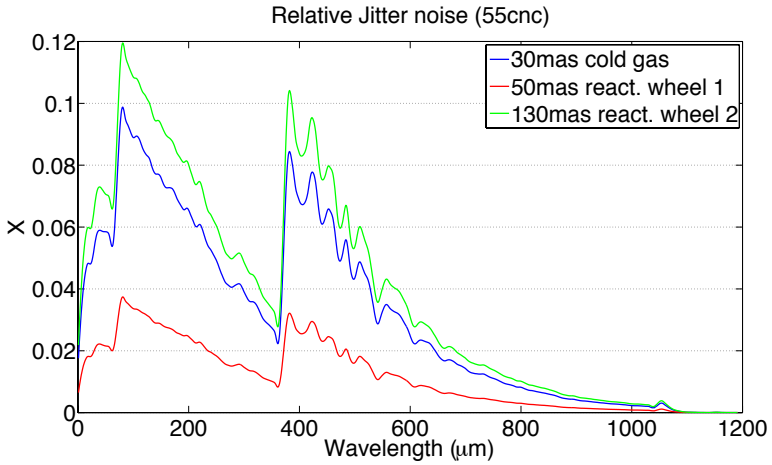

Figure 8: Excess noise variance as function of wavelength for the photon noise limited case (55 Cnc e). Here RPE and residual PRE noise after preliminary de-trending is shown. Blue: Cold Gas; Red: Reaction Wheel Option 1; Green: Reaction Wheel option 2.

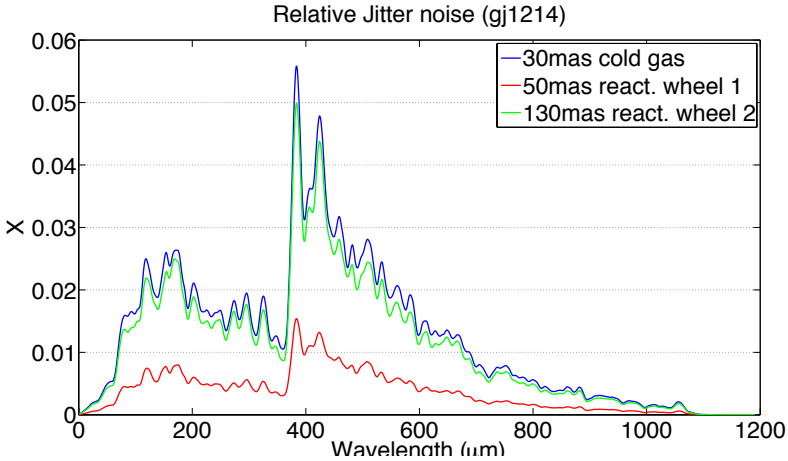

Figure 9: Excess noise variance as function of wavelength for the detector noise limited case (GJ1214b). Here RPE and residual PRE noise after preliminary de-trending is shown. Blue: Cold Gas; Red: Reaction Wheel Option 1; Green: Reaction Wheel option 2.

4.5 SUMMARY & INTERPRETATION

RPE Noise:

Within the scope of these simulations, we have considered a white power spectrum for RPE noise (> 1 Hz). Furthermore, RPE noise is not resolved by EChO and through integrating random high-frequency jitter, RPE noise is perceived as 'smearing' of the PSF across the detector focal plane. Due to the absence of more realistic jitter PSDs, we have only considered the effects of a flat RPE power spectrum.

For both cases (55 Cnc e and GJ1214b), we obtain results consistent with the initial considerations discussed in section 4.2. The 50 mas-rms reaction wheel option outperforms the cryo-jet 30 mas-rms solution. We can attribute this effect to an increased PSD at low frequencies and can draw the immediateconclusion that higher mas-rms are permissible (even preferable) if the overall spectral range of the RPE noise is larger. We find the 130 mas-rms reaction wheel option to perform worst in all cases.

RPE noise is most prominent in the blue part of the SWIR instrument. This is where the PSF is smallest and the effect of inter-, intra-pixel variations the strongest. Such effects can be mitigated with a slight de-focusing of the instrument.

RPE + PRE Noise:

Unlike high frequency RPE noise, low frequency PRE noise is resolved in a observation run by EChO. PRE noise manifests itself as wavelength and time correlated non-Gaussian systematic noise. Such noise can be mitigated in two ways: 1) parametrically and 2) non-parametrically.

In this tech note we investigate the effect of account for PRE noise using auxiliary centroiding information obtained from the FGS. We presented the residual noise in figures 8 and 9. We would like to utter a word of caution here: PRE noise is not fully removed using this simplistic de-trending step and requires the use of a full de-trending pipeline (not in the scope of this study). We hence consider the noise budgets in figures 8 and 9 as unrealistically pessimistic. Previous studies[3] have shown that with the use of advanced parametric and non-parametric techniques, it is possible to mitigate PRE noise on IR-detectors to within 10 – 30% of the photon noise budget (in this case the RPE noise budget).

[3]Swain et al. 2008 (Nature, vol. 452, p. 329), Waldmann et al. 2012 (ApJ, vol. 744, p. 35), Waldmann 2012 (ApJ, vol. 747, p. 12), Waldmann et al. 2013 (ApJ, vol. 766, p. 7), Waldmann 2013 (arXiv: 1301.2077v1).

5 PSF BREATHING

5.1 METHODOLOGY

We study here the effect of a time varying PSF arising from a coloured RPE spectrum and its associated instrumental photometric-gain variation. The usual three RPE cases are considered (table 1), which correspond to three different AOCS solutions.

NOTE: only the RPE contribution is considered in this analysis. PRE and MPE are neglected.

To model a coloured RPE spectrum, we used the following Brownian process assumption:

$$PS_{RPE}(f) = \begin{bmatrix} w^2\left[\left(\frac{f_0}{f}\right)^2 + 1\right] f_{min} < f < f_{max} \\ 0 \; otherwise \end{bmatrix}$$

where w is the white noise level, f_0 is the noise 'knee', and f_{min} and f_{max} define the spectral RPE band (see table).

A random pointing jitter timeline is generated assuming a Gaussian process with the above power spectrum. This random pointing jitter timeline is normalized to the RPE rms given in table 1.

5.2 RESULTS

Results vs the 1/f "knee" frequency are given in Figures 10 and 11.

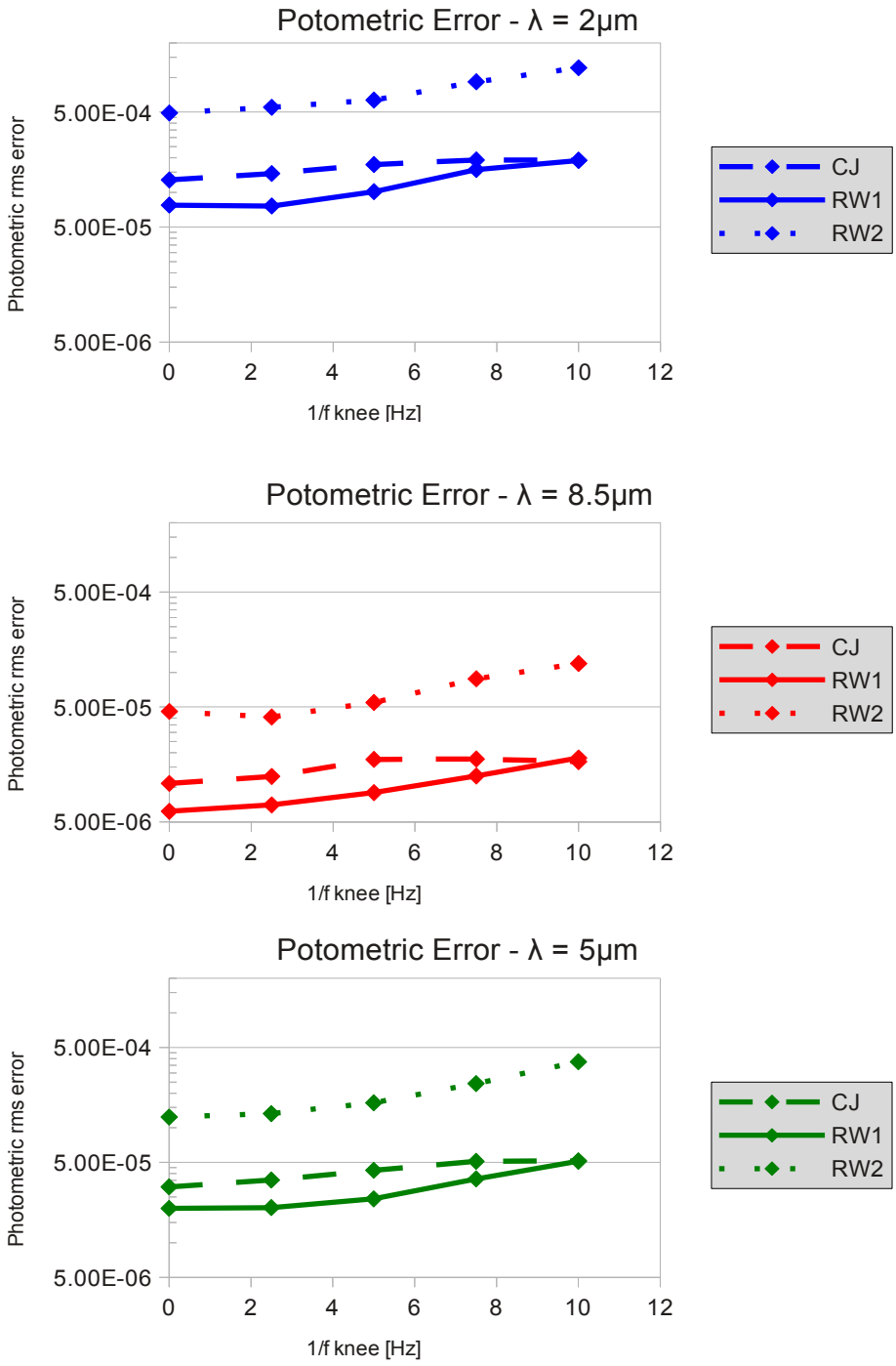

Figure 10: Effect of a RPE with a Brownian spectrum on the Photometric Error in 1 second of integration. Simulations are performed at 2, 5 and 8.5 μ m – blue, green and red curves, respectively. Cold-gas, RW1 and RW2 AOCS cases are given by the dashed, solid, and dotted curves, respectively (see legend). All plots on identical scale.

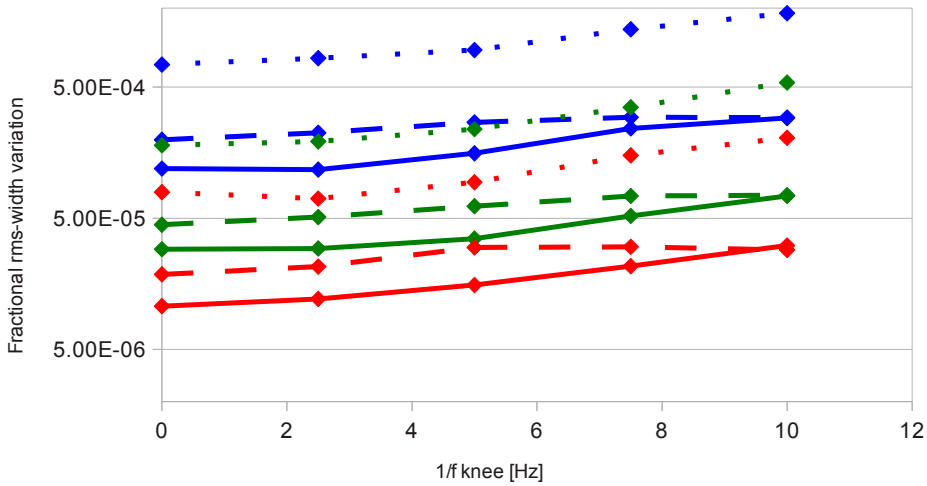

Figure 11:Effect of a RPE with a Brownian spectrum on the effective width of the PSF in 1 second of integration. See Figure 10 for a description of each curve.

5.3 SUMMARY & INTERPRETATION

Figures 10 and 11 show similar results for the PSF breathing as the RPE-PRE jitter in section 4: The 50 mas-rms reaction wheel optionconsistently outperforms (or is equivalent at 10 Hz) the cold gas option. The 130 mas-rms reaction wheel optionperforms worst for all frequencies considered. Overall we find that PSF breathing is a negligible effect in the relative noise error budget of EChO.

6 SUMMARY &CONCLUSION

In this tech note we have considered the impact of pointing jitter of the spacecraft on the photometric accuracy of the EChO mission. The pointing instability translates itself into photometric uncertainties via slit loss effects of dispersive channels, vignetting effect for fibre fed systems and inter-, intra-pixel gain variations of the detector.

Three pointing stabilisation options were considered: 1) Cryo Jets at 30 mas-rms RPE jitter, 2) Reaction wheels at 50 mas-rms RPE jitter and 3) Reaction wheels at 130 mas-rms RPE jitter. PRE jitter is assumed to be 20 mas-rms throughout.

We find that:

1) In all simulations considered, the 50 mas-rms RPE noise Reaction wheel option performs best in terms of photometric accuracy.
2) Photometric errors due to vignetting in the VNIR channel are negligible for all options and wavelengths.
3) Photometric errors resulting from PSF breathing effects are negligible for all channels and frequencies.
4) High frequency RPE noise is not resolved by EChO and in effect 'smears' the PSF as the jitter is integrated over time. This results in a distortion of the original PSF shape, which has to be taken into account at data reduction.
5) The effect of high frequency (RPE) noise for the MWIR and LWIR channels are negligible but photometric error amplitudes vary by up to an order of magnitude between the three options considered. Here the 50 mas-rms reaction wheel option performs best and the 130 mas-rms reaction wheel option worst.
6) RPE noise has the largest effect in the blue part of the SWIR channel(2.0 ~ 3.0μm). Current simulations are a worst-case scenario as the RPE noise distorted PSF is not taken into account at data reduction. We currently assume the SWIR design baseline of ~1.5 pixels FWHM in the spatial direction. The effect of RPE jitter in the SWIR channel can further be reduced by defocusing the PSF.
7) The effect of low frequency (PRE) noise is resolved in time by EChO. This systematic autocorrelative noise can be traced using pointing information derived by the FGS system. Ideal de-trending of time correlated time series noise is beyond the scope of this study. However we find a factor of 3 improvement using a FGS guided PSF extraction at data analysis. Previous studies show that PRE noise can be mitigated to within a few percent of the photon noise floor.